LARGE SYNOPTIC SURVEY TELESCOPE

Large Synoptic Survey Telescope (LSST)

LSST Crowded Fields photometry

K. Suberlak, C. Slater, Ž. Ivezić, P. Yoachim

LSST-2017

Latest Revision: 2018-01-25

revision: TBD
status: draft

Abstract

A report on the performance of current LSST Stack pipelines in crowded stellar fields. Using the real data we explore the metrics that could be used to direct decision-making process for pipeline improvements. The quality metrics show also a way to validate the performance of LSST pipelines after major software upgrades.

Change Record

Version	Date	Description	Owner name
1	2017-07-16	First draft.	Krzysztof Suberlak
2	2017-10-19	Updated outline.	Krzysztof Suberlak
2	2018-01-25	Major revision.	Krzysztof Suberlak

Contents

1 Introduction

We report on the performance of the Large Scale Synoptic Telescope (LSST) science pipelines [1], also known as 'the LSST stack', in stellar fields of varying levels of crowdedness.

The LSST will sample every night over 1,000 regions in the sky , delivering terabytes of raw data in need of processing: photometric and astrometric calibration, to deliver a calibrated exposure image, as well as a source catalog, among other image products[2] [3].

The survey sky is composed of regions very diverse in terms of stellar density, or crowdedness: from high density low-galactic latitude regions that have tens of millions of sources per square degree, to low-density regions towards the galactic poles with less than thousand sources per square degree.

Deblending and successful photometry is an inherent part of any astronomical data processing pipeline. There exists a body of research answering questions that are specific to crowded stellar fields, eg. how many beams do we need per source (see [2]), or how the crowded fields photometry can be approached in the era of large telescopes [4] Other studies involved eg. HyperSuprime CAM pipeline (developed in parallel with the LSST Stack), recognizing that the deeper the survey, the higher the stellar densities encountered, and the onset of blurring the the boundaries between deblending, measurement, and detection [1].

In this report we compare the 'out-of-the-box' LSST Stack tools, in particular processCcd.py, to the DECAm [Galactic] Plane Survey (DECAPS) catalogs based on the NOAO state-of-the-art community pipeline ([5]). First we use the LSST Metrics Analysis Framework Galfast simulation of the night sky find regions representing various stellar densities - see Sec. 2. Then we query the DECAPS image database for images that were taken at exposures and filters that reach similar depth to the LSST single-visit depth (Sec. 3). We select few DECAPS exposures at each density level, and process with LSST Stack tools (Sec. **??**). In Sec. **??** we compare the results of LSST processing and the DECAPS single-epoch catalogs, and develop the quality metrics. Finally in Sec. **??** we make recommendations for future work.

---

[1]`https://pipelines.lsst.io`
[2]`http://ls.st/LSE-163`

2   Identifying density regions

To identify regions representing different stellar densities we use the LSST Metrics Analysis Framework [3] simulated stellar density map prepared by P. Yoachim and L. Jones [4]

The resulting dataset `starDensity_r_nside_64.npz` contains 64 magnitude bins, with the entire sky divided into 49152 healpixels [5]. Each healpixel contains information about the number of stars per square degree in a given magnitude bin in the simulated sky - see Fig. 1.
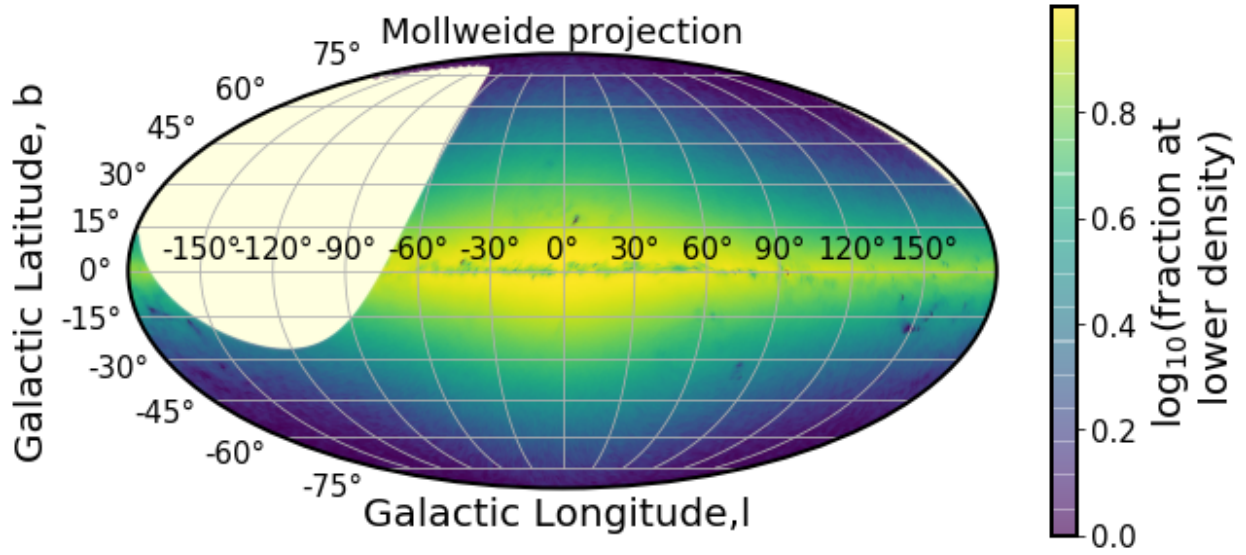

FIGURE 1: MAF healpixels plotted in galactic coordinates in Mollweide projection. The brightest regions correspond to highest stellar densities. The missing part in the higher declination is the part of the sky above $\delta > 40°$, which is not observable from the southern location of Cerro Pachón.

To match the LSST single-visit depth, we select magnitude bins smaller than r=24.5. For each healpixel we calculate the number of pixels that have a higher stellar count. Since each healpixel has an equal area, the fraction of pixel number above a certain threshold corresponds to the fraction of sky area above given density limit. Fig. 2 illustrates how we define percentiles of stellar densities, so that eg. 'top 1%' density means that only 1 in 100 pixels has a higher density than a given pixel, and 'top 10%' means that '10 %' of pixels in the considered simulation of the sky.

---

[3] `https://www.lsst.org/scientists/simulations/maf`, and `https://github.com/lsst/sims_maf`
[4] `sims_maf/python/lsst/sims/maf/maps/createStarDensitymap.py`
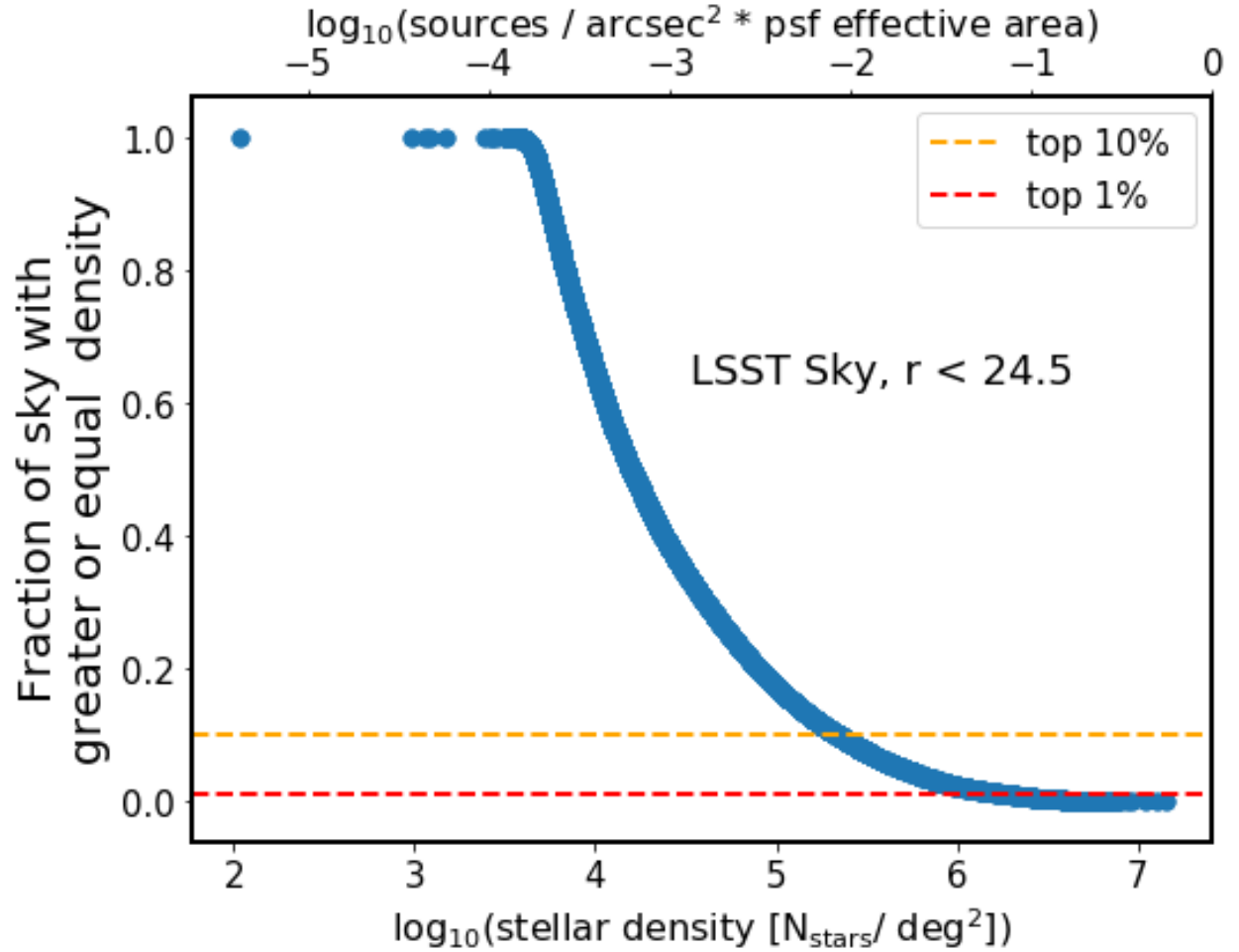[5] `http://healpix.sourceforge.net`

FIGURE 2: We order all healpixels in the MAF simulation of LSST sky in terms of stellar count per pixel. For each healpixel we calculate the number of pixels at greater or equal stellar count, which corresponds to the area of the sky at greater density. Normalizing that by the total number of pixels we obtain a fraction of the sky at greater or equal density, similar to the cumulative distribution. Horizontal dashed lines illustrate selecting pixels at 5% or 10% density.

Since this definition of density includes all pixels that are within 'top 20%', we take selection around the percentiles so that :

- top 1 % means fraction of sky with greater density is 0.01

- 5 % region means such that between 4% and 6%

- 20 % region includes 19% - 21%

- 50 % region includes 49% - 51%

We illustrate the location of pixels representative of these density brackets on the sky in Fig. 3.
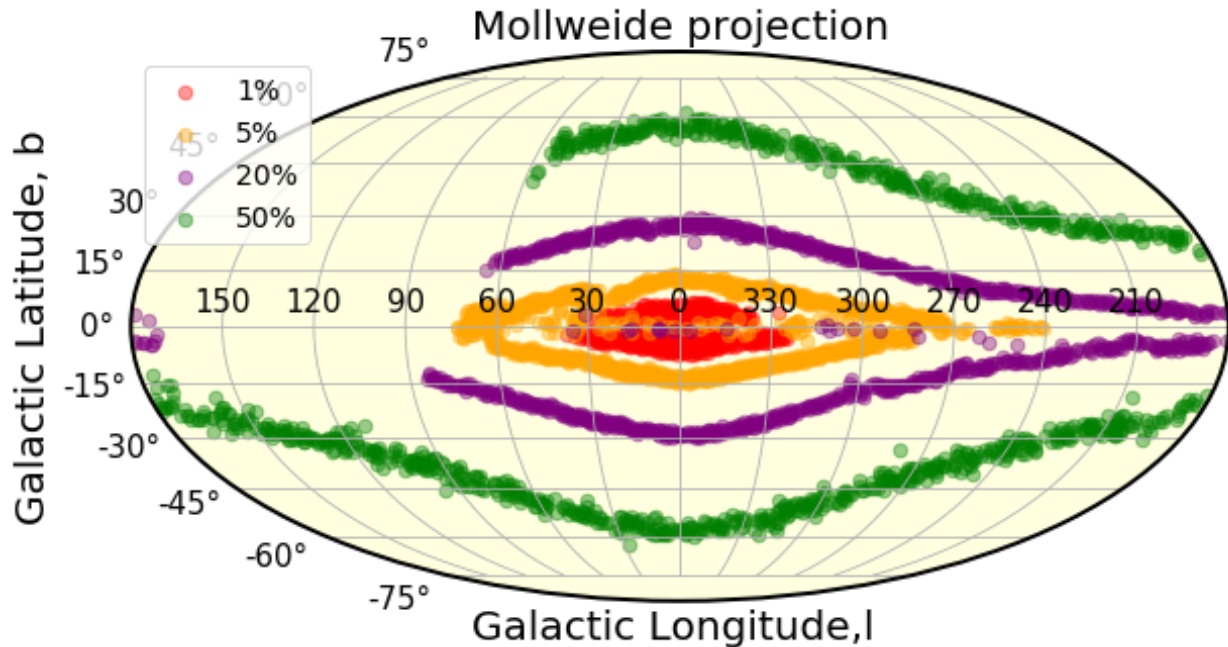

FIGURE 3: Illustration of location of regions representative of different relative density in cylindrical projection, galactic coordinates. The highest density regions are located close to the galactic bulge, and the decreasing density regions approximately trace isophotes of the Milky Way. The 20% regions close to the galactic equator correspond to high extinction regions that appear to have less counts due to interstellar dust.

3 DECam Plane Survey

We compare the MAF estimates of stellar density in various density regimes to Dark Energy Camera (DECam) data, taken with the 4-m Cerro Tololo Inter-American Observatory telescope

(CTIO)[6]. To circumvent lack of possibiliy of querying by a list of coordinates at the NOAO Data Archive [7], we used the SQL query. We first obtained all data that fulfilled very loose criteria:

- telescope = 'ct4m'

- instrument = 'decam'

- 90 sec < exposure < 125 sec

- release_date < '2017-07-24'

- dec < 0

- proctype = 'InstCal'

- prodtype = 'image'

- filter is u, g, r, or VR

(the exact SQL query used is available in the Appendix A.1). The exposure time was chosen to match the LSST depth at 30 second exposure.

We obtained 11928 rows (individual fields) fulfilling these criteria. The location of these observations on the sky, with overlaid MAF density regions, is shown on Fig. 4.

We used AstroPy SkyCoord package to match the coordinates of MAF healpixels to DECam imaging data. For instance, of the 244 healpixels in the top 1% density regime 91 had a DECam counterpart within 30 arcminutes. We allowed very liberal bounds to only approximately point at the same region of the sky - see Fig. 5.

3.1   DAOStarFinder source detection

Per each density regime, we selected five random DECam fields, and performed source extraction with DAOStarFinder[8]. This tool uses a classic DAOFIND algorithm [7], and we used it to verify the plausibility of the MAF source densities using real data. DECam employs mosaic CCDs - each field, which can be downloaded as a fits.fz compressed file, is split into 60 primary

---

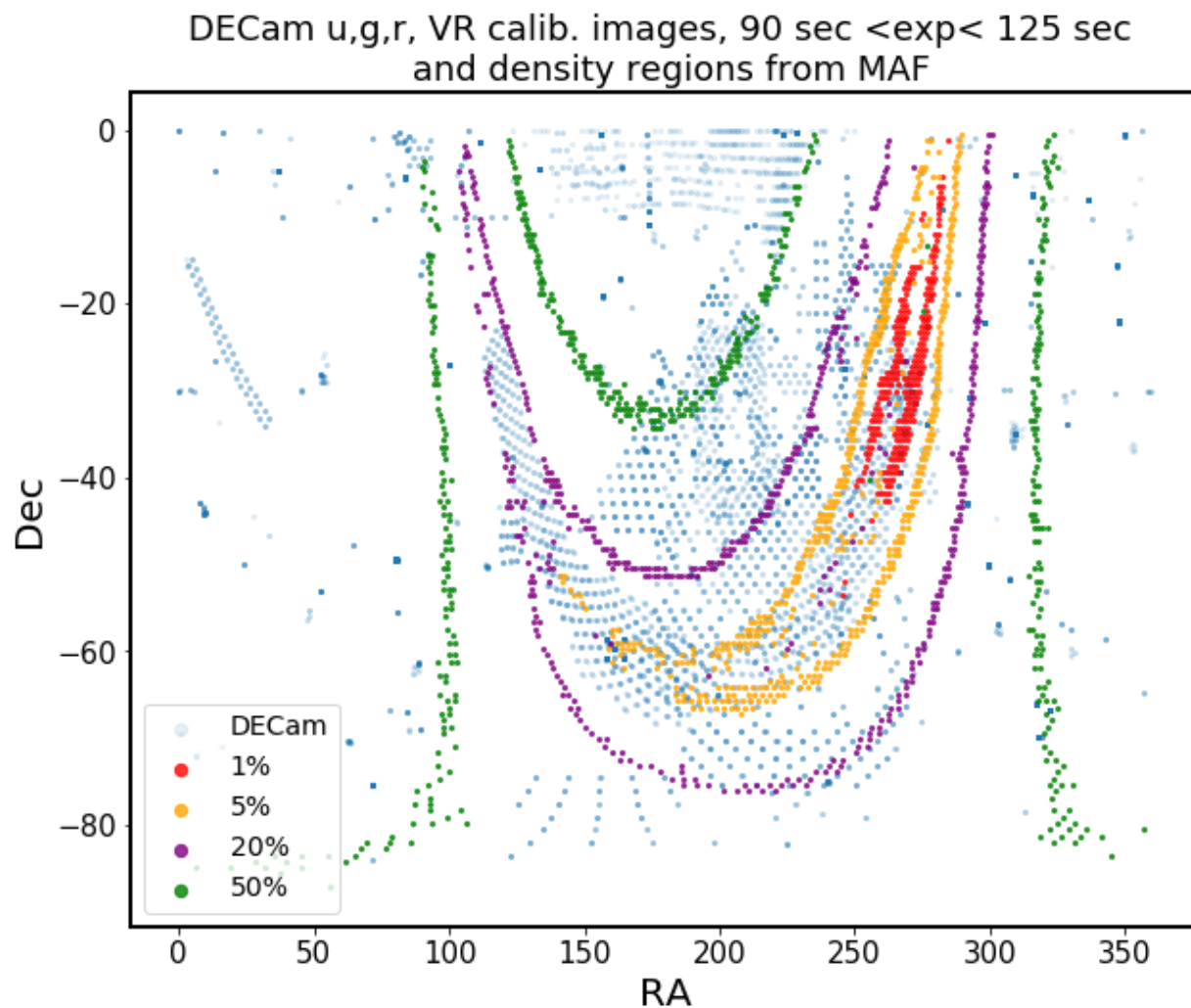[6]see `http://www.ctio.noao.edu/noao/node/1033`
[7]`http://archive.noao.edu/search/query`
[8]`http://photutils.readthedocs.io/en/stable/photutils/detection.html`

FIGURE 4: DECam observations with exposure $\in [90, 125]$ sec, $\delta < 0$, taken in u,g,r, or VR filter.
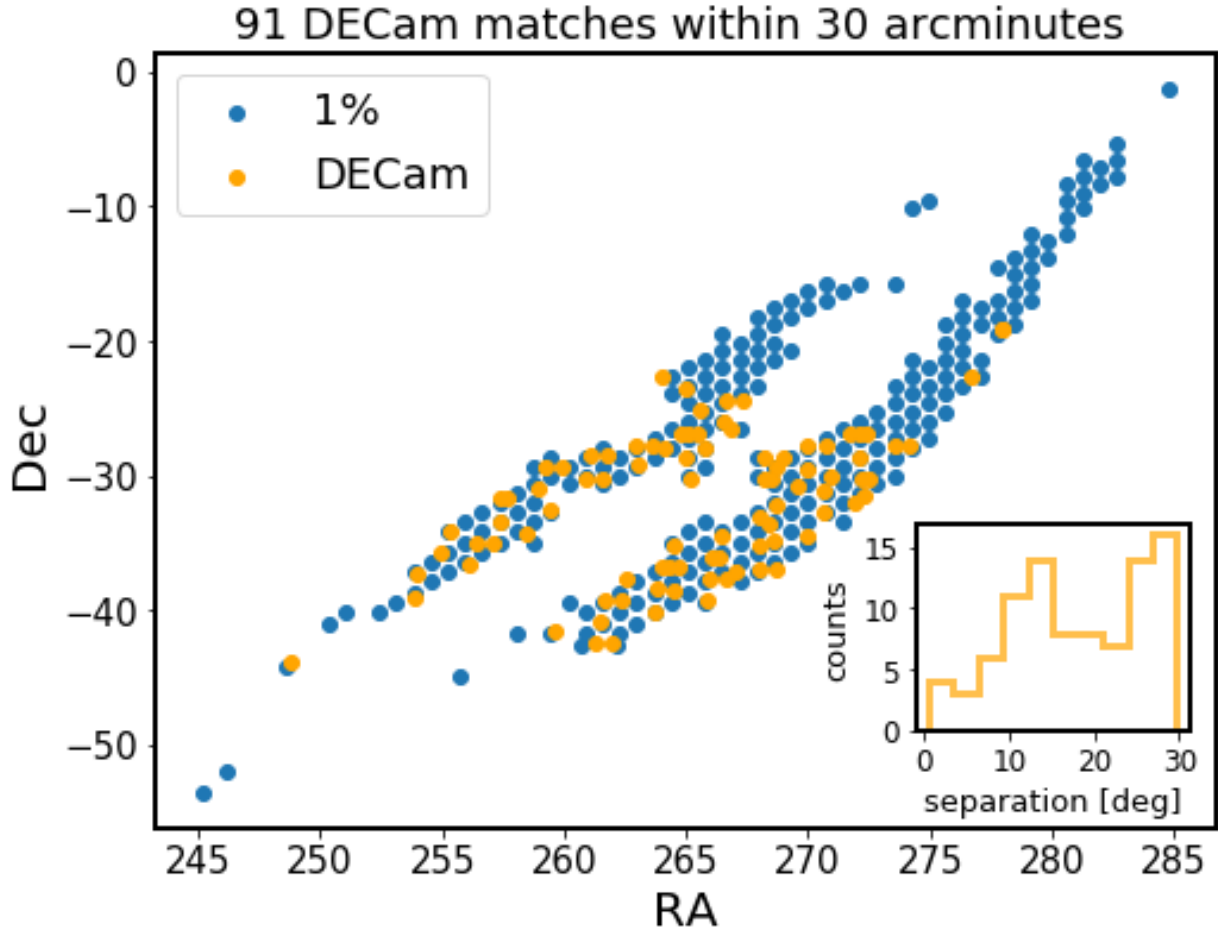
FIGURE 5: DECam observations with exposure $\in [90, 125]$ sec, $\delta < 0$, taken in u,g,r, or VR filter, matched using 2D separation to MAF healpixels within the highest stellar density bins. The inset shows the distribution of separation between healpix coordinates and DECam image center. Each DECam image is a mosaic of CCDs, and each mosaic element covers approximately 9x18 arcminutes (see Fig. 6 for illustration).
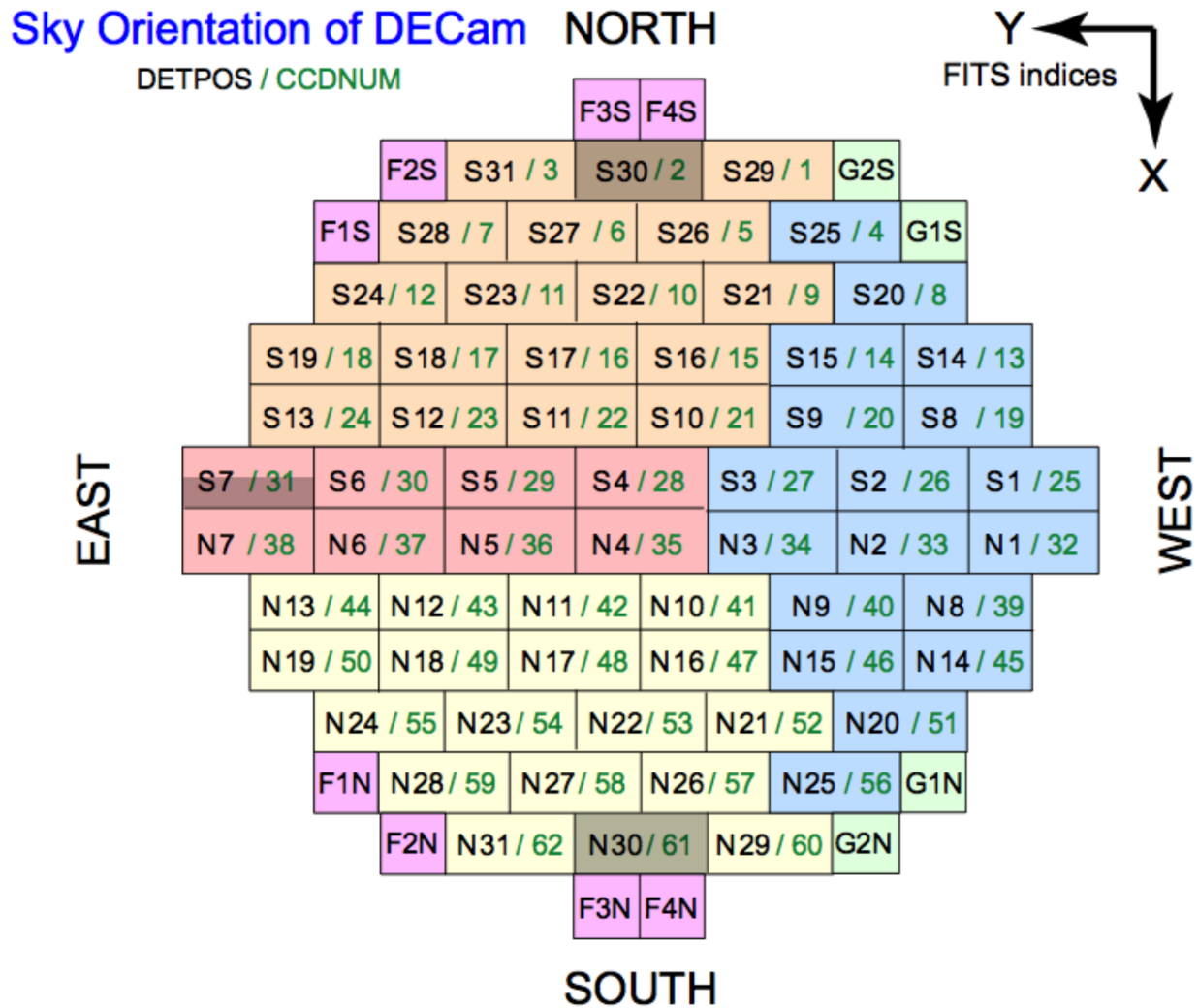
FIGURE 6: An illustration of the DECam CCD mosaic image plane, adapted from [6], Fig.4-3. The color corresponds to the one of the four sets of read-out electronics (orange,pink, blue,yellow), or the guiding (green) and focus (magenta) CCDS. The grey CCDs do not function properly. In using the LSST Stack processing we used CCD10 (S22) or CCD11 (S23) (for astrometric comparison).

archive	l	b	TRILEGAL	MAF	DAO
c4d_140624_080728_ooi_r	13.70	-4.43	7,960,511	2,650,680	498,760
c4d_170428_094150_ooi_g	356.86	-3.90	39,852,793	4,587,804	375,980
c4d_170501_055757_ooi_g	356.26	5.05	16,352,821	2,659,968	285,630
c4d_170504_084722_ooi_g	4.26	5.15	15,586,874	2,833,740	561,795

TABLE 2: Source density comparison for 1% density level : TRILEGAL, DAO and MAF columns contain stellar counts from TRILEGAL simulation , DAOStarFinder based on DECam data, and MAF simulation, respectively. Simulation results are limited by LSST r < 24.5. All counts are in stars per square degree.

HDUs. FITS viewing software, such as ds9, by default open the first element (HDU[1]), and we decided to perform source extraction on this one element of the mosaic per field, since each element is of the same size, and is equally representative of the field. The size of each element of the mosaic is 2046x4094 pixels, with pixel scale of 0.27 arcsec / px , so that a single mosaic element covers an area of 0.047117 sq.deg. Using the FWHM information from the FITS header, and sigma clipped standard deviation σ, we performed source extraction with the detection threshold at 5σ level, setting the detection threshold at 5σ, and scaled it up to the source count per square degree to allow comparison with MAF data.

3.2 TRILEGAL queries

We also obtained TRILEGAL[9] simulation results for each of the DECam fields, submitting to the online form the DECam ra,dec, and field size (using the size of a single mosaic element, as for DAOStarFinder source extraction - approximately 0.047117 sq.deg. per field). We limited the query results selecting r < 24.5 with LSST ugrizy photometric system, keeping all other settings as default.

3.3 Comparison of MAF, DAOStarFinder, and TRILEGAL counts

We used the number of sources per TRILEGAL output file, and scaled it to the degree level to compare with MAF and DAO. The results are shown in Tables 2, 3 , 4 , 5 for 1%,5%,20% and 50 % density levels.

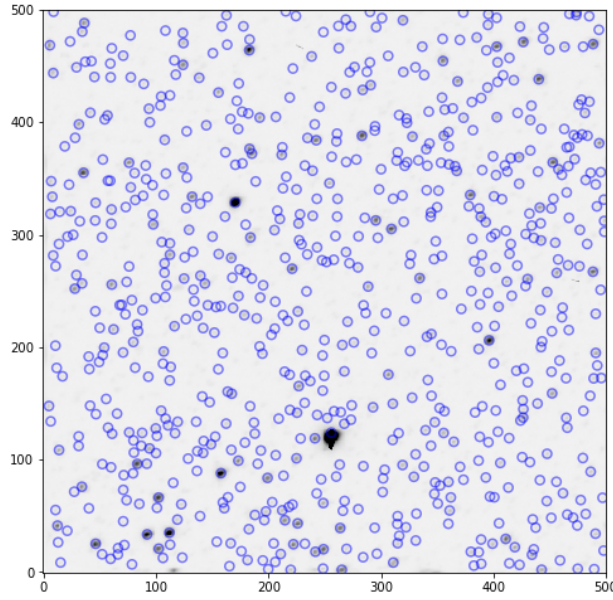[9] http://stev.oapd.inaf.it/cgi-bin/trilegal

FIGURE 7: 500x500 pixels (135x135 arc-seconds) subregion of DECam field c4d_170504_084722_ooi_g, a top 1% density region. With DAOPhot threshold set at 5 σ, we detected 722 sources in this postage stamp miniature, corresponding to the area of 0.001406 sq degrees, which translates to 513,422 sources per square degree. At the same coordinates, MAF density is 2,833,740 sources per square degree, and TRILEGAL density is 15,586,874 sources per square degree.
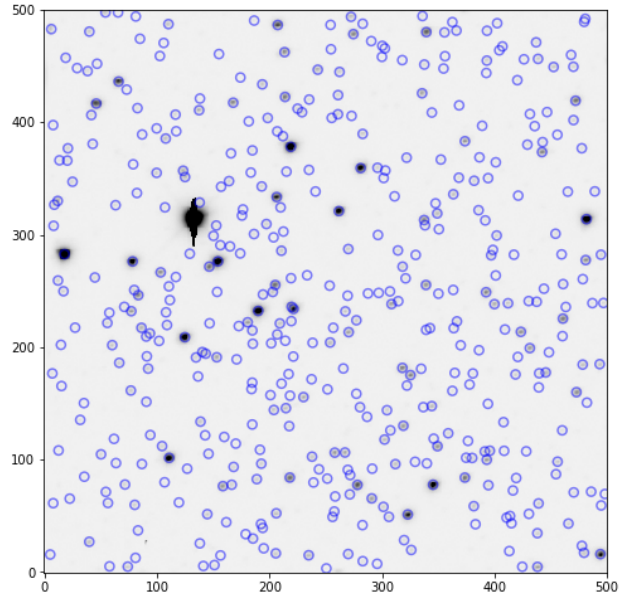
FIGURE 8: 500x500 pixels (135x135 arc-seconds) subregion of DECam field c4d_170429_035748_ooi_g, with 436 detected sources, in the 5 % density region. The same DAOPhot settings as Fig. 7. That many sources in an area of 0.001406 sq degrees, translates to 310,044 sources per square degree. At the same coordinates, MAF density is 807,156 sources per square degree, and TRILEGAL density is 1,870,414 sources per square degree.

archive	l	b	TRILEGAL	MAF	DAO
c4d_160316_065235_ooi_g	301.42	3.40	1,606,135	591,336	179,277
c4d_160825_231905_ooi_g	314.05	3.08	2,564,964	589,572	127,088
c4d_170429_035748_ooi_g	310.43	-4.02	1,870,414	807,156	327,483
tu1677011	4.48	8.70	2,530,163	810,144	509,093

TABLE 3: Source density comparison for 5% density level, all columns and units as in Table 2

archive	l	b	TRILEGAL	MAF	DAO
c4d_170122_055542_ooi_g	242.43	3.77	341,343	116,856	66,282
tu1661798	351.66	20.42	183,778	118,188	44,216
tu1668579	217.04	1.21	379,319	111,096	54,004
tu2187073	312.84	14.64	184,583	107,784	60,678

TABLE 4: Source density comparison for 20% density level, all columns and units as in Table 2
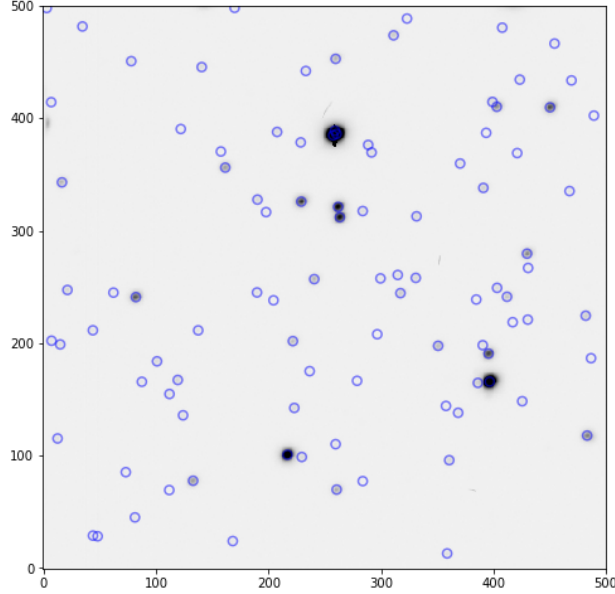
FIGURE 9: 500x500 pixels (135x135 arc-seconds) subregion of DECam field c4d_170122_055542_ooi_g, with 98 detected sources, in the 20 % density region. The same DAOPhot settings as Fig. 7. That many sources in an area of 0.001406 sq degrees, translates to 69,688 sources per square degree. At the same coordinates, MAF density is 116,856 sources per square degree, and TRILEGAL density is 341,343 sources per square degree.
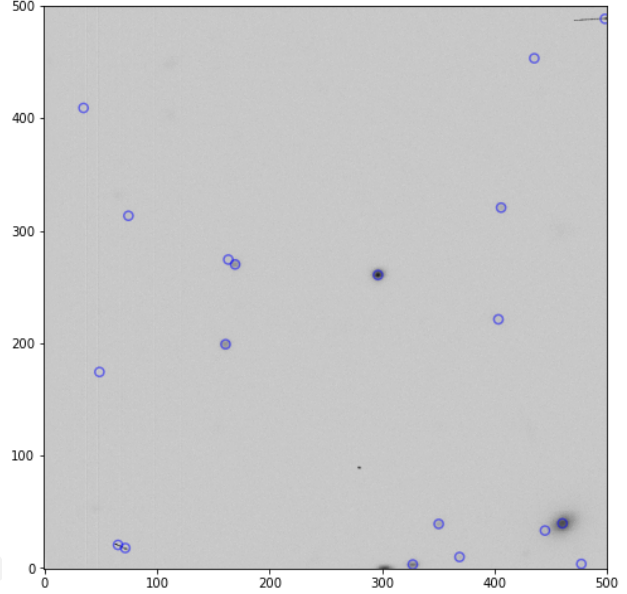
FIGURE 10: 500x500 pixels (135x135 arcseconds) subregion of DECam field c4d_160607_025052_ooi_g, with 19 detected sources, in the 50 % density region. The same DAOPhot settings as Fig. 7. That many sources in an area of 0.001406 sq degrees, translates to 13,511 sources per square degree. At the same coordinates, MAF density is 20,052 per square degree, and TRILEGAL density is 29,607 sources per square degree.

archive	l	b	TRILEGAL	MAF	DAO
c4d_150615_005257_ooi_g	344.39	41.67	27,633	21,024	12,904
c4d_160607_025052_ooi_g	2.92	41.68	29,607	20,052	13,371
c4d_160825_034122_ooi_g	345.83	1.28	18,364,268	20,268	91,177
tu2046406.fits.fz	220.89	-16.08	41,832	19,944	35,974

TABLE 5: Source density comparison for 50% density level, all columns and units as in Table 2

4   Performance of the LSST Stack

We conducted more detailed studies of the LSST Stack performance. For each case there is a source catalog considered as ground 'truth', and images at various stellar densities that were processed with the LSST Stack.

We aim to answerr the following questions:

- how does the completeness vs. magnitude curve depend on the input source density (expressed in terms of the dimensionless parameter that takes seeing into account) ?

- how does the photometric error (rms for true minus measured mag) vs. mag curve depend on the input source density?

4.1   LSST Stack on DECam

First we compared the DECaPS individual image catalogs[10], which were made using iterative source detection (see [5]), and the LSST source catalogs, based on the DECAm images.

We chose DECam fields representative of 20% , 5%, and 1% level stellar densites. Querying the NOAO Archive against the field coordinates and exposure range we obtained instcal, wtmap, and dqmask per field. Using the staging functionality of the public ftp we downloaded these files onto the NCSA lsst-dev01 machine. We processed each image with `obs_decam` tools, specifically `ingestImagesDecam.py`, and `processCcd.py`. We analyzed the source catalogs and calibrated images. Using the 20% region in g filter, 96-sec exposure and r-filter 50 sec exposure we constructed CMD diagram to demonstrate the functionality of photometric accuracy. We demonstrated astrometric accuracy by using the 20% region 96-second exposure in r-filter, and processing CCD10 and CCD11 - there is no overlap in the position of detected sources along the CCD boundary, which confirms that there is no major problem with astrometry.

---

[10]`http://decaps.skymaps.info/`

4.2 LSST Stack on StarFast

Second, we employed the StarFast image simulator[11], that simulates the volume with randomly distributed known population of stars. We simulated stellar densities equivalent to 20%, 5% , and 1% regions, comparing the StarFast input catalogs to the source catalogs resulting from the LSST Stack processing of simulated images.

5 Conclusions

A Appendix : SQL queries

A.1 NOAO DECam query

```
SELECT \
  reference, dtpropid, surveyid, release_date, start_date, \
  date_obs, dtpi, ra, dec, telescope, instrument, filter, \
  exposure, obstype, obsmode, proctype, prodtype, seeing, \
  depth, dtacqnam, filesize, md5sum, \
  reference AS archive_file
FROM \
  voi.siap \
WHERE \
  ((exposure > 90) AND (exposure <125 ) )  \
AND release_date < '2017−07−24' \
AND (dec <= 0) \
AND (proctype = 'InstCal') \
AND (prodtype = 'image') \
AND (telescope = 'ct4m') \
AND (instrument = 'decam') \
AND ((filter ILIKE 'u DECam%' ) \
OR (filter ILIKE '%g DECam%' ) \
OR (filter ILIKE '%r DECam%' ) \
OR (filter ILIKE '%VR DECam%' ) ) \
ORDER BY date_obs ASC LIMIT 250000
```

---

[11] https://dmtn-012.lsst.io

References

[1] Bosch, J., et al. 2017, ArXiv e-prints

[2] Hogg, D. W. 2001, The Astronomical Journal, 121, 1207

[3] Narayan, G., et al. 2018, ArXiv e-prints

[4] Olsen, K. A. G., Blum, R. D., & Rigaut, F. 2003, AJ, 126, 452

[5] Schlafly, E. F., et al. 2017, ArXiv e-prints

[6] Shaw, R. A. 2015, NOAO Data Handbook

[7] Stetson, P. B. 1987, PASP, 99, 191